Extended Abstracts of the 1996 International Conference on Solid State Devices and Materials, Yokohama, 1996, pp. 16-18

A New Observation of the Reverse Short Channel Effect in Submicron n-MOSFET by Using Gate-Induced Drain Leakage Current Measurement

*S. M . Cheng , Steve S. Chung, and M. S. Liang**

Department of Electronic Engineering, National Chiao Tung University, Hsinchu , Taiwan, R.O.C.
**Taiwan Semiconductor Manufacturing Co., Hsinchu Science-based Industrial Park., Hsinchu, Taiwan, R.O.C.*

In this paper, a significant channel length dependence of the drain leakage current and its degradation is investigated for the first time in submicron n-MOSFET's. This phenomenon is attributed to the increase of lateral nonuniform channel doping concentration near the source/drain sides as a result of the process-induced boron redistribution effect. It is visible for devices with increasing channel doping near the source/drain sides due to oxidation-enhanced diffusion (OED) or process-induced implant damages as the channel length decreases. A simple band-to-band tunneling model and numerical simulation are used to verify this channel length dependent behavior.

1. Introduction

An anomalous increase in the threshold voltage V_T with decreasing channel length, called the Reserve-Short-Channel Effect (RSCE), has been commonly attributed to the laterally nonuniform channel profile [1-3]. For the direct verification of RSCE, in addition to observe it from the V_T-L curve [1] or conventional C-V method [4], there is no direct evidence to show the existence of the lateral non-uniform channel doping along the channel. Only until recently, we have demonstrated it based on a charge-pumping measurement [5]. In this paper, we will for the first time propose *a different while simple approach* to observe the above nonuniform doping effect based on GIDL(Gate Induced Drain Leakage) current [6] measurement. Furthermore, the increase of effective channel doping concentration as a function of channel length is determined by using a simple band-to-band tunneling model and the length dependence of GIDL characteristics is verified by using 2D simulation.

2. Experimental: Channel Length dependent GIDL Current

Two types of n-channel MOS devices were fabricated in this study. The V_T implant is 110 Kev, 2 x 10^{12} cm^{-2} BF_2 for type A and 25 Kev, 3 x 10^{12} cm^{-2} for type B devices. The thickness of gate oxide was 140 nm for type A and 7 nm for type B devices. After gate patterning, the arsenic was implanted at an energy of 80 Kev and a dose of 5 x 10^{15} cm^{-3} to form the n^+ source/drain for two devices. Fig. 1 shows the measured V_T as a function of the channel length for type A and B devices which both show reverse short channel effect. Fig. 2 and Fig. 3 show the measured GIDL current characteristics. The drain leakage currents are strongly affected by substrate bias for both devices, but only channel length dependent for type A devices was observed. The length dependence of type A is quite different from the previous report [6-7], in which the drain leakage current is independent of the channel length. Moreover, the current degradation $\Delta I_D/I_D$ versus time for type A is also length dependent as observed in Fig. 4.

3. Verification of RSCE: the Model and Simulation

The lateral nonuniform channel doping concentration near the source/drain is believed to contribute to the length dependence of the measured GIDL and current degradation characteristics. Fig. 5 shows the schematic diagram of the increasing channel doping concentration near the drain region for short and long channel devices. An analytical model and simulation are used to verify the above arguments as follows. Equations listed in Table 1 are used to calculate the normal field E_n and lateral field E_l, in which V_{FB} is the flat-band voltage, ϕ_S is the surface potential where tunneling occurs, N_D represents the effective drain doping concentration, respectively. The model parameters A, B are extracted from the intersection and the slope of each line by using the characteristics of $\log(I_D/E_T^2)$ vs $1/E_T$.

In order to determine the effective channel concentration N_{eff} near the drain, we assume the fitting parameters A and B extracted from long channel devices are also valid for short channel devices. Under such an assumption, the value of N_{eff} can be obtained for various channel length devices by using the equations listed in Table 1. The extracted effective channel doping concentrations of type A devices are shown in Fig. 6, N_{eff} is increasing as the channel length decreases and is beyond 1 x 10^{17} cm^{-3}. We believe that the lateral field at the corner for type A devices can become sufficiently large such that the GIDL current will be dependent on the N_{eff} near the drain. This result confirms the above observation that GIDL currents are enhanced for short channel devices. The extracted effective channel doping concentration near the drain of type B is below 1 x 10^{17} cm^{-3} but almost the same for various channel lengths (not shown in Fig. 6) such that the length dependence of GIDL currents is less significant than for type A devices.

To verify the observed RSCE, a simple model and simulations have been made. Fig. 7 shows the calculated results and measured data for type A devices with various

channel lengths, in which good agreement is observed. The simulations of channel doping along the channel direction of type A and B are also demonstrated in Fig. 8, in which oxidation-enhanced diffusion (OED) and transient-enhanced diffusion (TED) models [8-9] were used in the simulation. The OED effect is dominant in type A devices, while TED effect is dominant in type B devices. We found that the doping concentration near the drain of type A is higher than that of type B and is consistent with the above observations. The simulated GIDL currents of type A and B are also shown in Fig. 9, in which channel length dependent is obtained for type A devices and channel length independent for type B devices. To describe the discrepencies, simulations of the electric field for type A and B devices were compared as shown in Figs. 10(a) and (b) respectively. We observed that the total field of short channel length device is higher than long channel length device in type A devices, such that the channel length dependent current was observed. For type B devices, the total field is almost the same for various channel lengths so the current is channel length independent.

Moreover, according to the increase of effective channel doping concentration near the drain region devices, the increase of lateral field with the reducing channel length will be obtained. This is the reason why the off-state degradation of type A is more severe than that of type B devices and has a length dependent feature.

4. Conclusion

A new approach to observe the S/D implant or process-induced RSCE using GIDL measurement is proposed. The channel length dependent GIDL current is visible for the devices with the increasing effective channel doping concentration near the drain due to the OED as the channel length decreases. In contrast, this behavior was not observed for devices (such as type B) with TED. In the current method, it provides us a convenient way to characterize the non-uniform channel doping in the current submicron and deep-submicron MOS devices. The channel length dependent behavior of GIDL current shows a great impact on the further scaling of ULSI applications, in particular nonvolatile memories, since GIDL current can not be scaled with device dimension.

Acknowledgements This work was sponsored by the National Science Council under contract *NSC84-2215-E009-075* and in part by the Tsmc, Hsinchu Science-based Industrial Park, Taiwan.

References

1) M. Orlowski *et al.*, in *IEDM Tech. Dig.*, p. 632, 1987.
2) C. Y. Lu *et al.*, *IEEE EDL.*, EDL-10, p. 446, 1989.
3) T. Kunikiyo *et al.*, *IEEE Trans.* CAD-13, p. 507, 1994.
4) C. Y. Chang et al., *IEEE EDL*, vol. 15, p. 437, 1994.
5) S. S. Chung et al., in *Symp. VLSI Tech.*, p. 103, 1995.
6) J. Chen et al., *IEEE EDL, vol. EDL-8*, p. 515, 1987.
7) C. Chang and J. Lien, in *IEDM Tech. Dig.*, p.714, 1987.
8) User's Manual of ATHENA: 2D Process Simulation Framework, *SILVACO international*, March 1994.
9) User's Manual of ATALS: 2D Device Simulation Framework, *SILVACO international*, March 1994.

$$I_D = AE_T^2 \exp(-B/E_T) \quad (1)$$

where

$$E_T = \sqrt{E_n^2 + E_l^2} \quad (2)$$

$$E_l = \sqrt{2qN_{eff}/\varepsilon_{si}}\sqrt{V_{BI}+V_{DB}} \quad (3)$$

$$E_n = (V_{DB} + V_{FB} - \phi_s)/(3T_{ox}) \quad (4)$$

$$\phi_s = K_o - \sqrt{K_o^2 - V_{DG}^2} \quad (5)$$

and

$$K_o = V_{DG} + (qN_D T_{ox}^2 \varepsilon_{si})/\varepsilon_{ox}^2. \quad (6)$$

Table 1 Analytical model of the GIDL current

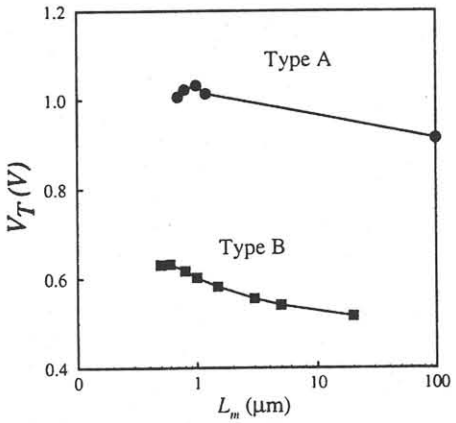

Fig. 1 Measured threshold voltage versus channel length for type A and type B devices.

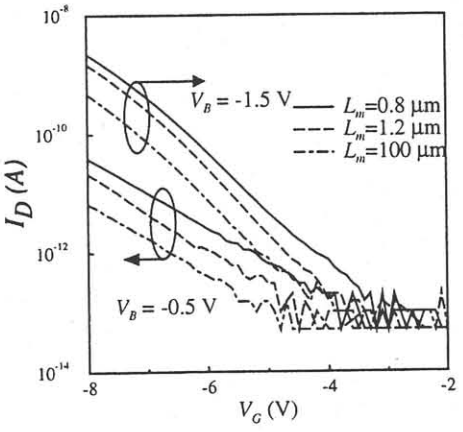

Fig. 2 Measured leakage current (GIDL) for type A MOSFET's with various channel lengths, in which length-dependent feature is observed.

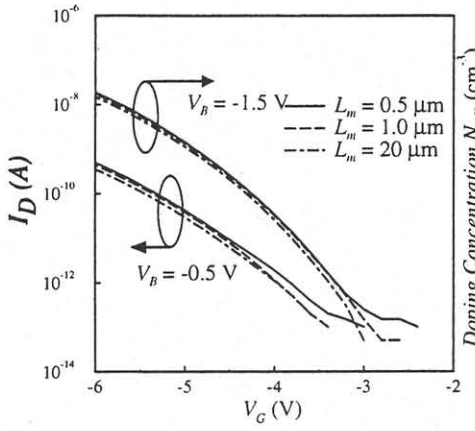

Fig. 3 Measured GIDL current for type B devices with various channel lengths. GIDL is independent of the device channel length.

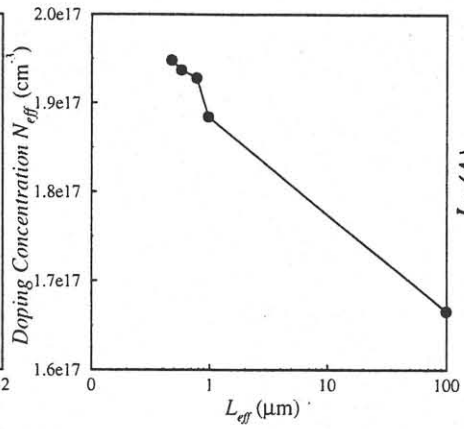

Fig. 6 Effective channel doping concentration N_{eff} near the drain region as function of channel length for type A devices as calculated from Eq. (3).

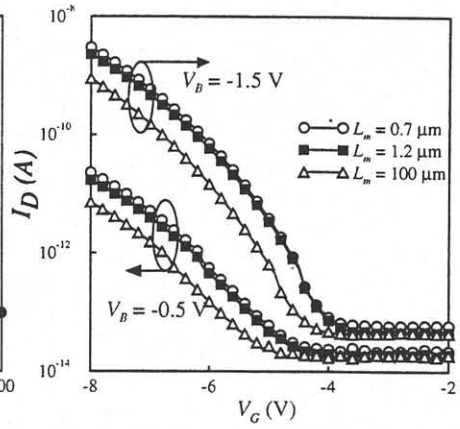

Fig. 9 The simulated GIDL currents characteristics for various channel length type A devices. They are consistent with those measured data in Fig.2.

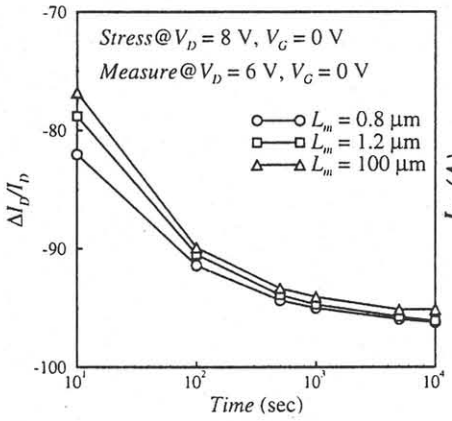

Fig. 4 Drain current degradation of type A devices stressed under off-state biases V_D = 8V and V_G = 0 V. Channel length dependent feature is also shown.

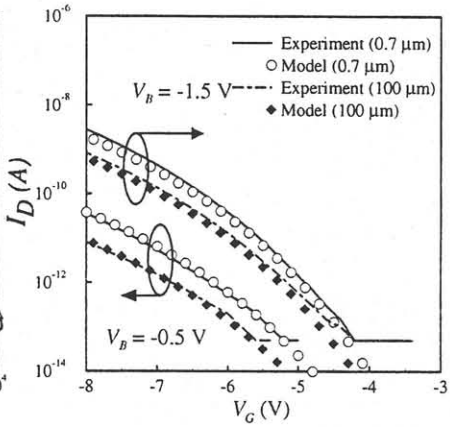

Fig.7 Comparison of GIDL current characteristics between experiment and model for type A devices with channel lengths of 0.7 μm and 100 μm. Lines show measured data and symbols show calculated results.

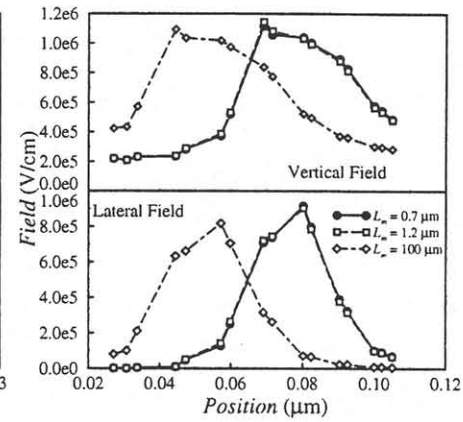

Fig.10 Simulated maximum lateral and vertical fields for various channel length devices in type A.

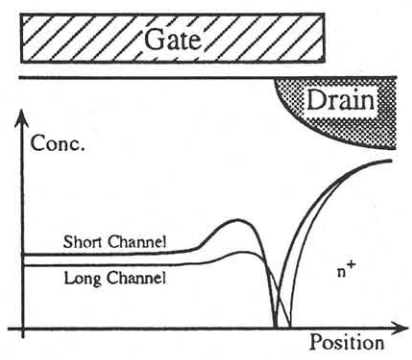

Fig. 5 Schematic diagram of the channel doping concentration near the drain region for short and long channel devices with reverse short channel effects.

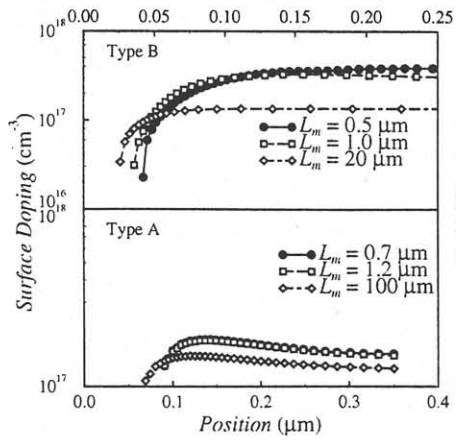

Fig. 8 Simulated lateral surface doping concentrations for type A and type B devices.

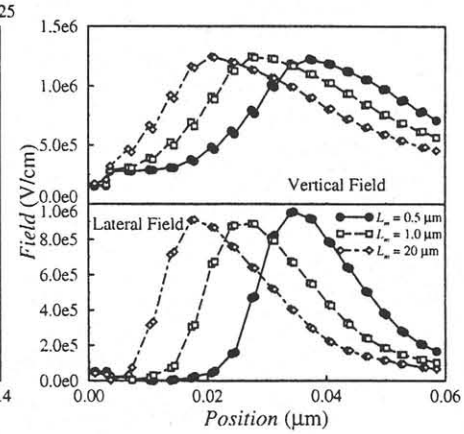

Fig.11 Simulated maximum lateral and vertical fields for various channel length devices in type B.